CFD simulations to study the effects of wall protrusions on microfluidic mixing

2015 J. Micromech. Microeng. 25 084008

(http://iopscience.iop.org/0960-1317/25/8/084008)

IOP Publishing Journal of Micromechanics and Microengineering
J. Micromech. Microeng. **25** (2015) 084008 (14pp) doi:10.1088/0960-1317/25/8/084008

CFD simulations to study the effects of wall protrusions on microfluidic mixing

Sourav Sarkar[1], K K Singh[2], V Shankar[1] and K T Shenoy[2]

[1] Department of Chemical Engineering, Indian Institute of Technology, Kanpur 208016, India
[2] Chemical Engineering Division, Bhabha Atomic Research Centre, Trombay, Mumbai 400085, India

E-mail: kksingh@barc.gov.in

Received 2 March 2015, revised 17 April 2015
Accepted for publication 5 May 2015
Published 22 July 2015

Abstract

In this study the effects of different types of wall protrusions on microfluidic mixing are studied using computational fluid dynamics (CFD) simulations. Two new protrusions, single first bracket protrusions and double opposite first bracket protrusions (DOFBPs), are conceptualized, evaluated through CFD simulations and compared to protrusions having standard geometrical shapes, e.g. rectangular protrusions, triangular protrusions and semicircular protrusions. In the range of Reynolds numbers covered in this study, the microchannel having an opposed T-junction and DOFBPs is found to provide good mixing. A hybrid approach relying on the modification of microfluidic junctions as well as wall protrusions for enhancing microfluidic mixing is also evaluated. The microchannel based on the hybrid approach of an OA 10°–20°–165° WY-junction and DOFBPs is also found to provide very good mixing for a wide range of Reynolds numbers.

Keywords: microchannel, microfluidics, mixing, micromixer, CFD, protrusions

(Some figures may appear in colour only in the online journal)

Notation

c	Concentration ($\mathrm{mol\,m^{-3}}$)
c_0	Concentration at inlet ($\mathrm{mol\,m^{-3}}$)
c_i	Concentration at ith cell in the cross section of interest ($\mathrm{mol\,m^{-3}}$)
$\bar{c}$	Average concentration in the cross section of interest ($\mathrm{mol\,m^{-3}}$)
D_{AB}	Diffusivity of binary mixture of A and B ($\mathrm{m^2\,s^{-1}}$)
i	Index of cell
MI	Mixing index (−)
MI_T	Mixing index for the microchannel with an opposed T-junction with straight layout (−)
$\vec{N}$	Molar flux ($\mathrm{mol\,m^{-2}\,s^{-1}}$)
$\hat{n}$	Unit vector representing outward normal to a boundary/surface
p	Pressure (Pa)
p_0	Pressure at outlet (Pa)
ΔP	Pressure drop in a microchannel (Pa)
ΔP_T	Pressure drop in a microchannel with an opposed T-junction with straight layout (Pa)
$\vec{v}$	Velocity vector ($\mathrm{m\,s^{-1}}$)
v_0	Average velocity at inlet ($\mathrm{m\,s^{-1}}$)

Greek Symbols

η	Number of nodes in the cross section of interest
μ	Dynamic viscosity (Pa s)
υ	Kinematic viscosity ($\mathrm{m^2\,s^{-1}}$)
ρ	Density ($\mathrm{kg\,m^{-3}}$)
σ^2	Variance of concentration ($\mathrm{mol^2\,m^{-6}}$)
σ^2_{max}	Maximum variance of concentration ($\mathrm{mol^2\,m^{-6}}$)

Abbreviations

CFD	computational fluid dynamics
DOFBP	double opposite first bracket protrusion
RP	rectangular protrusion
SCP	semicircular protrusion
SFBP	single first bracket protrusion
TP	triangular protrusion
TZP	trapezoidal protrusion

1. Introduction

Chemical processing in microchannels offers several advantages such as intensified heat transfer, high specific interfacial area and very small inventories. Due to these advantages chemical processing in microchannels has found numerous applications such as fast exothermic chemical reactions (de Mello *et al* 2004, Waterkamp *et al* 2007, Cvjetko and Žnidaršič-Plazl 2011, Sen *et al* 2013), gas–liquid mass transfer (Yue *et al* 2007), liquid–liquid mass transfer (Zhao *et al* 2007, Darekar *et al* 2014a, Sen *et al* 2014), reactions coupled with mass transfer (Bhoi *et al* 2014) and reactions involving hazardous or toxic chemicals (Hessel *et al* 2005). Scaling up to realize a high throughput is also relatively easy (Kikutani *et al* 2002, Iwasaki *et al* 2006, Saber *et al* 2010, Darekar *et al* 2014b). Though there are several advantages to chemical processing in microchannels, mixing in microchannels is a challenge which needs to be addressed if microchannels are to be used for carrying out fast reactions. As the characteristic diameters of microchannels are very small, flow in microchannels is usually laminar. In laminar flow mixing is mainly dependent on molecular diffusion and hence is slow. If reactions are to be carried out in a microchannel, good mixing of reactants is a prerequisite. If methods are not devised to improve microfluidic mixing, the performance of a microchannel for a reaction or unit operation may not be as expected. Consequently, enhancement of mixing in microchannels has been an active area of research.

Different approaches to improve microfluidic mixing can be classified into two broad categories—modification of the geometry of the microchannel and externally induced mixing. There exists a vast literature on the enhancement of microfluidic mixing using modifications of geometry. Mengeaud *et al* (2002) carried out 2D simulations to study mixing in a zigzag microchannel with a Y-junction. It was observed that below a critical Reynolds number (Re ~ 80), mixing was governed by molecular diffusion but for higher Reynolds numbers recirculation in laminar flow contributed to mixing. Soleymani *et al* (2008) carried out experimental and numerical studies on microfluidic mixing. They studied the effects of flow rate, the angle between the two inlet channels and aspect ratio on microfluidic mixing. They also studied mixing in microchannels with new types of junctions such as the throttle junction, TT-junction and TT-junction with circular obstructions. The microchannel with a TT-junction with circular obstructions was found to provide better mixing than the microchannel with a simple T-junction. Sheu *et al* (2012) proposed a new design for a planar micromixer which had curved microchannels with tapered cross-section and split and recombine structures. Split and recombine action coupled with Dean vortices induced by curvature were found to enhance mixing. Nonino *et al* (2009) performed numerical simulations to compare mixing in microchannels with different layouts. The microchannels compared were planar zigzag, curvilinear and square-wave microchannels. Among the three microchannels, the curvilinear microchannel was found to be the best. Alam and Kim (2012) performed numerical simulations to evaluate the performance of a curved microchannel with an opposed T-junction. The walls of the microchannels had outward protrusions (rectangular grooves). The mixing index was found to depend on the width of the grooves but not on the depth of the grooves. Fang *et al* (2012) used numerical simulations and experiments to study the effect of providing mixing units in a T-junction microchannel with an otherwise straight layout. The mixing unit consisted of a square chamber with two baffles for bending the flow path. The results obtained from 2D simulations showed that 28 such mixing units were required to achieve good mixing. Sahu *et al* (2013) carried out numerical simulations and experiments to study the effect of providing inward rectangular protrusions (RPs) on microfluidic mixing. Two arrangements of protrusions—symmetric and staggered—were compared. The mixing performance of both types of protrusions was similar but the pressure drop was less for the staggered arrangement of protrusions.

In the second category, i.e. externally induced microfluidic mixing, methods such as pulsatile flow, ultrasonic waves and electrokinetic instabilities have been used. Glasgow and Aubry (2003) studied the effect on mixing of using pulsating flow in a T-junction microchannel. Mixing was found to be the best when both flows were pulsed out of phase. Yaralioglu *et al* (2004) integrated piezoelectric transducers in a microchannel and used ultrasonic waves to enhance microfluidic mixing. Oddy *et al* (2001) used electrokinetic instability to enhance microfluidic mixing.

Apart from the studies focusing on modification of geometry and studies focusing on externally induced microfluidic mixing, there are several studies which focus on general aspects of microfluidic mixing, e.g. the effect of the Reyolds number on mixing and the accuracy of numerical simulations in the prediction of microfluidic mixing. Engler *et al* (2004) carried out experimental studies on opposed T-junction microchannels and identified three different flow regimes—stratified laminar flow at low Reynolds numbers (Re ~ 7), vortex flow at intermediate Reynolds numbers (Re ~ 60) and engulfment flow at high Reynolds numbers (Re ~ 199). The onset of engulfment flow was observed to provide a sudden increase in mixing. Bothe *et al* (2006) studied mixing in T-junction microchannels using computational fluid dynamics (CFD). Adeosun and Lawal (2009) studied residence time distributions in T-junction microchannels and used residence time distributions to indirectly characterize flow and mixing in microchannels. Liu (2011) studied mixing of a scalar due to convection and diffusion in a non-planar micromixer using CFD. The effect of false diffusion on the solution of the scalar transport equation was studied. A range of molecular diffusivities, which cover most of the liquid solutions of interest, in which false diffusion is smaller than molecular diffusion is found to exist. In this range the scalar transport equation can be solved accurately using CFD. Wong *et al* (2004) studied mixing in T-junction microchannels fabricated in silicon. Mixing was studied with the help of a blue dye and following the hydrolysis reaction of dichloroacetyl phenol red. Mixing was found to be good in the range of Reynolds numbers from 400 to 500.

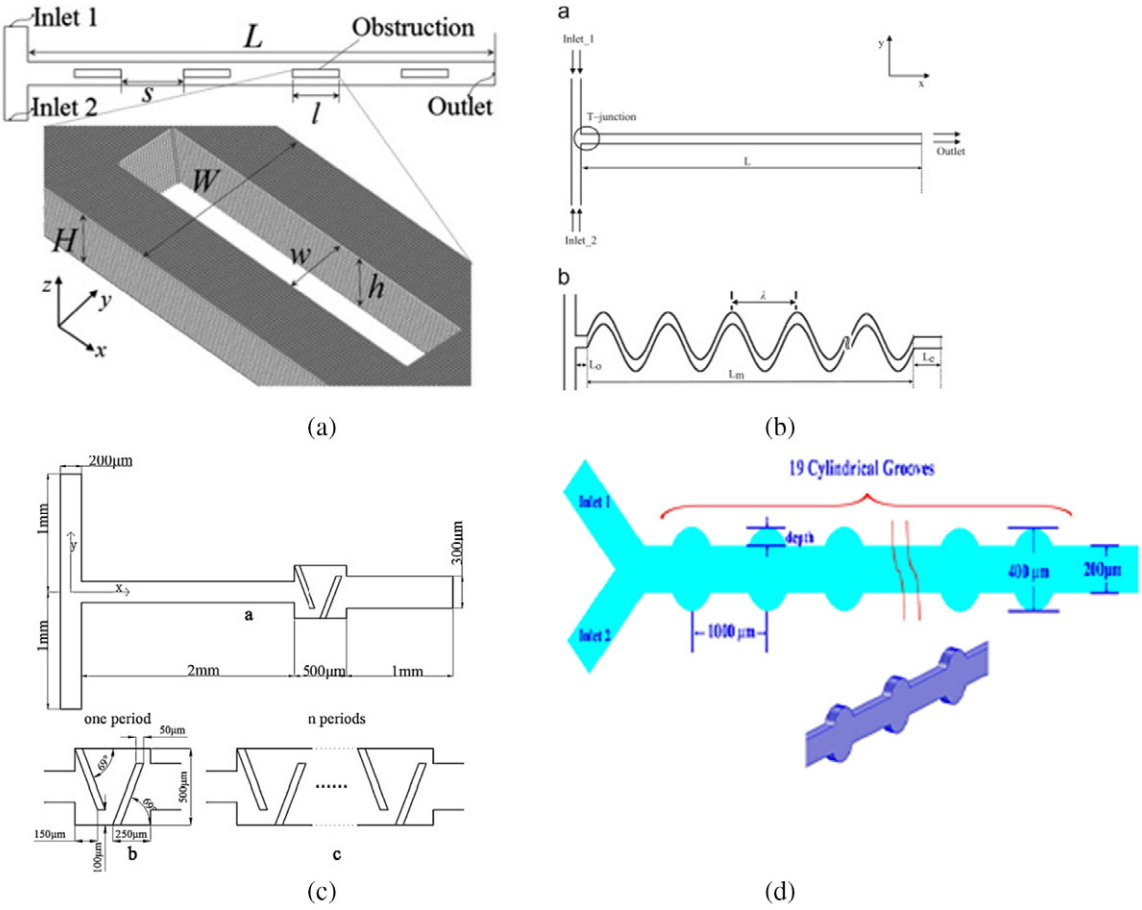

Figure 1. Different approaches for modifying the layout of a microchannel to improve microfluidic mixing. (a) Modifying the layout using obstacles in the flow path. Reprinted with permission from Leung and Ren (2013). Copyright 2013 Elsevier. (b) Modifying a straight layout to a zigzag layout. Reprinted with permission from Afzal and Kim (2014). Copyright 2014 Elsevier. (c) Modifying the layout using inward wall protrusions. Reprinted with permission from Fang *et al* (2012). Copyright 2012 Elsevier. (d) Modifying the layout using outward wall protrusions. Reprinted with permission from Wang *et al* (2015). Copyright 2015 Wiley.

The literature on microfluidic mixing is too vast to cover in this section. The reader is referred to several review papers which provide summaries of different studies on microfluidic mixing (Ottino and Wiggins 2004, Nguyen and Wu 2005, Suh and Kang 2010, Capretto *et al* 2011).

The approach of modifying the geometry to improve microfluidic mixing can be further classified into two categories—modification of the microfluidic junction (Soleymani *et al* 2008, Sarkar *et al* 2014) and modification of the layout of the microchannel (Mengeaud *et al* 2002, Soleymani *et al* 2008, Nonino *et al* 2009, Sheu *et al* 2012, Alam and Kim 2012, Fang *et al* 2012, Sahu *et al* 2013). In our previous work (Sarkar *et al* 2014) we studied the modification of microfluidic junctions to improve microfluidic mixing. Modifying the geometry by modifying the layout of the microchannel to improve mixing is the subject of this study. The ways of modifying the layout of a microchannel can be further classified into four classes, as shown in figure 1. These are putting obstacles in the flow path (Soleymani *et al* 2008, Leung and Ren 2013), providing zigzag (tortuous) flow paths (Mengeaud *et al* 2002, Nonino *et al* 2009, Sheu *et al* 2012, Afzal and Kim 2014), providing inward wall protrusions (Fang *et al* 2012, Sahu *et al* 2013) and providing outward wall protrusions (Alam and Kim 2012, Wang *et al* 2015). In this study we focus on mixing induced by inward wall protrusions and use CFD as a virtual prototyping tool to evaluate some conventional and some new designs of inward wall protrusions.

Modification of geometry to achieve process intensification, in particular enhancement of heat transfer, is not new as the idea has been reported in several studies. For example, Khodadadi *et al* (1986) studied the enhancement of the Nusselt number in laminar forced convective heat transfer in a 2D 90° bifurcation using numerical simulations. Dipprey and Sabersky (1963) carried out experiments to study the enhancement of heat transfer in rough tubes with granular type roughness. Similarly, Webb (1971) studied the effect of repeated rib-roughness on heat transfer and pressure drop for turbulent flow in tubes. Gee (1980) studied the heat transfer and pressure drop characteristics of helically rib-roughened tubes. Nguyen *et al* (1989) studied heat transfer and pressure drop in tubes roughened with an internal circumferential rib. The rough tubes used in these studies are akin to smooth tubes with different types of inward wall protrusions and in that sense the idea of using inward wall protrusions for intensification of transport processes is quite old.

2. Computational approach

2.1. Governing equations

The computational approach used in this study involves numerical solution of the Navier–Stokes and convection–diffusion equations as applicable for steady-state flow of an incompressible fluid. These equations are:

$$\nabla \cdot \vec{v} = 0 \tag{1}$$

$$\vec{v} \cdot \nabla \vec{v} = -\frac{1}{\rho} \nabla p + \upsilon \nabla^2 \vec{v} \tag{2}$$

$$\vec{v} \cdot \nabla c = D_{\mathrm{AB}} \nabla^2 c. \tag{3}$$

Here $\vec{v}$ is the velocity vector D_{AB} is the molecular diffusivity and c is the concentration of the solute. For all the simulations density ρ and viscosity μ are kept constant at 998.2 kg m^{-3} and 0.00103 Pa s (that of liquid water at room temperature). Molecular diffusivity is maintained as 10^{-9} m^2 s^{-1}. The commercial solver COMSOL Multiphysics 4.2 is used to carry out the numerical simulations.

2.2. Boundary conditions

The boundary conditions at the inlets can mathematically be written as:

$$\vec{v} = -v_0 \hat{n} \tag{4}$$

$$c = c_0 \tag{5}$$

where appropriate values are assigned to v_0 and c_0 in the simulations. No slip and zero flux conditions are used at the walls of the microchannels. These boundary conditions can be written as:

$$\vec{v} = 0 \tag{6}$$

$$-\hat{n}\vec{N} = 0 \tag{7}$$

where $\vec{N}$ represents the flux of the species being mixed and it is the sum of the convective and diffusive flux. The expression for $\vec{N}$ is given by the following equation:

$$\vec{N} = (c\vec{v} - D_{\mathrm{AB}} \nabla c). \tag{8}$$

The pressure outlet and convective flux boundary conditions are used at the outlet for the momentum transport and mass transport equations, respectively. The relevant equations are:

$$p = p_0 = 0; \mu\{\nabla \vec{v} + (\nabla \vec{v})^T\} \cdot \hat{n} = 0 \tag{9}$$

$$-\hat{n} \cdot D_{\mathrm{AB}} \nabla c = 0. \tag{10}$$

2.3. Quantification of mixing

As reported in several other studies on mixing in microchannels (Soleymani *et al* 2008, Alam and Kim 2012, Sarkar *et al* 2014) mixing is quantified using a mixing index defined as

$$\mathrm{MI} = \left(1 - \sqrt{\frac{\sigma^2}{\sigma^2_{\max}}}\right) \times 100 \tag{11}$$

$$\sigma^2 = \frac{1}{\eta} \sum_{i=1}^{\eta} (c_i - \bar{c})^2. \tag{12}$$

Unit feed concentration is considered in the simulations. c_i is the concentration at the ith node of the mesh at the outlet face, $\bar{c}$ is the average concentration at the outlet face and η is the number of nodes at the outlet face. σ^2 and $\sigma^2_{\max}$ denote the actual variance and maximum possible variance at the outlet, respectively. $\sigma^2_{\max}$ is calculated by taking $\bar{c}$ equal to 0.5 while c_i is kept as 0 for half of the cross-section and 1 for the remaining half. Thus value of $\sigma^2_{\max}$ is 0.25. MI, the mixing index, can have a maximum value of 100 representing complete mixing ($c_i = 0.5$, $\sigma^2 = 0$) and a minimum value of 0 ($\sigma^2 = \sigma^2_{\max}$) indicating no mixing.

2.4. Grid independence test

The grid size used in this study is based on the grid independence test reported in our previous study (Sarkar *et al* 2014). The number of cells was varied from less than 1 million to 4 million and the effect of the number of cells on the pressure drop and mixing index was tracked. Microchannels of two different geometries were used to carrying out the grid independence test. A grid consisting of about 3 million cells was found to be sufficient. A similar grid quality has been used in the simulations reported in this study.

2.5. Validation

The computational approach adopted in this work has been validated as described in detail in our previous study (Sarkar *et al* 2014). Validation was carried out by comparing the predictions of the numerical simulations with both experimental data and analytical results. In the experiments the interface between the two liquid streams (water and dyed water) being mixed in a Y-junction microchannel was tracked at a fixed axial distance from the junction for different values of flow rate ratios of the two streams. The interface between the streams could also be tracked in the simulations. Good agreement between the location of the interface predicted by the simulations and observed in the experiments was found, as shown in figure 2.

To validate the computational approach using analytical results, the variation of the transverse diffusion length with axial distance for a T-junction, as predicted by simulations, was measured. The variation of predicted transverse diffusion zone thickness with axial distance is shown in figure 3.The thickness of the transverse diffusion zone predicted by the simulation was found to have a power law dependence on the axial distance with an exponent equal to 0.454. This value of the exponent is very close to the analytical result which predicts the exponent to be 0.5.

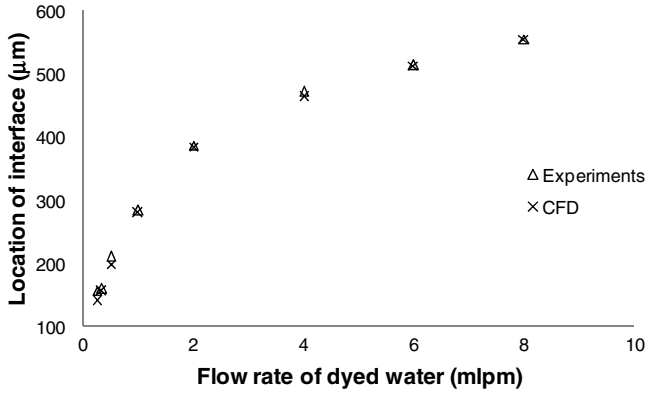

Figure 2. Location of the interface between the dyed water and the water streams measured at a distance of one channel diameter from the junction. The location specifies the distance in the cross-flow direction, measured from the side of the dyed water. The water flow rate is 2 mlpm.

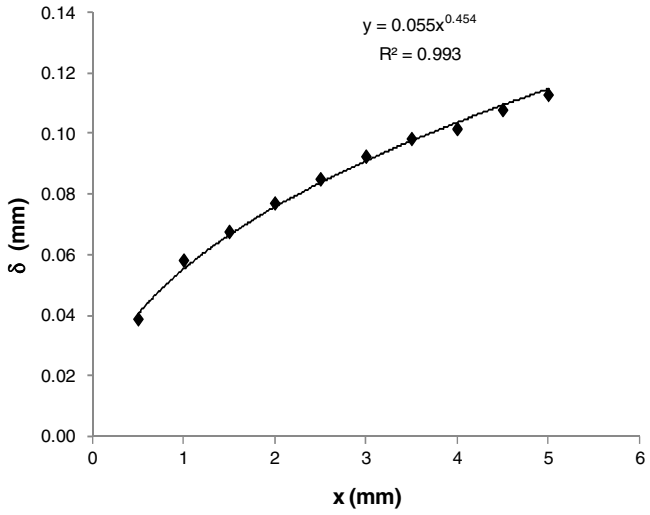

Figure 3. Variation of transverse diffusion zone thickness with axial distance in the microchannel with an opposed T-junction at Re = 50.

The validation of the computational approach based on experimental observations and analytical results gives us confidence that the computational approach used in this study can be used to predict the mixing performance of microchannels with different types of inward wall protrusions.

3. Results and discussion

3.1. Inward protrusions with standard geometrical shapes

To begin with the mixing performance of microchannels with inward protrusions of standard geometrical shapes, e.g. rectangles, triangles and semicircles, were evaluated. A rectangular shape is one of the most commonly used shapes of wall protrusions or bends. Wong *et al* (2003) and Sahu *et al* (2012) studied mixing in microchannels with rectangular bends. In this study, a microchannel with an opposed T-junction (depth 0.5 mm, width 0.5 mm and junction to outlet and inlet to inlet length 5 mm) with inward rectangular protrusions (RPs) is considered. The RPs are 0.3 mm high, 0.5 mm deep and 0.25 mm wide. The distance of the first protrusion from the junction is 1 mm and the center to center distance of two adjacent protrusions is 0.5 mm. The top view of the microchannel with six RPs and the streamlines predicted from the CFD simulations are shown in figure 4(a). The velocity vectors around the RPs are shown in figure 4(b). Another standard geometrical shape that can be used as an inward wall protrusion to modify the layout of a microchannel is the triangular shape. The top view of the microchannel with an opposed T-junction and six triangular protrusions (TPs) is shown in figure 4(c). The protrusions are made of equilateral triangles 0.3 mm in height. The first TP is at a distance of 1 mm from the junction and the center to center distance between two protrusions is 0.5 mm. The velocity vectors around the TPs are shown in figure 4(d). The third standard geometry of inward wall protrusion evaluated is the semicircle. A T-junction microchannel with semicircular protrusions (SCPs) is evaluated. The radius of a SCP is 0.3 mm. The centers of the SCPs coincide with the wall. The first SCP is 1 mm away from the junction and the center to center distance between two adjacent SCPs is 0.5 mm. The top view of the microchannel with an opposed T-junction with six SCPs and its streamlines are shown in figure 4(e). The streamlines shown in figure 4 give the impression that there are dead zones present in the corners of the microchannels. But a careful look at the velocity vectors given along with the streamlines reveals that these are not dead zones but zones of recirculation. The mixing indices and pressure drops for three microchannels with RPs, TPs and SCPs are summarized in table 1. Table 1 also lists the mixing index and pressure drop in a T-junction microchannel with no wall protrusion for comparison. The fourth column of table 1 lists the ratio of pressure drop in a microchannel and pressure drop in a T-junction microchannel with a straight layout. The fifth column lists the ratio of the mixing index in a microchannel and the mixing index in a T-junction microchannel with a straight layout. The concentration profiles at the outlets of the microchannels are shown in figure 5. As is evident from table 1 and figure 5, providing wall protrusions enhances mixing significantly as all three microchannels with wall protrusions are found to have much better mixing than the microchannel without wall protrusions. Among the three wall protrusions evaluated, SCPs are found to provide the best mixing followed by RPs, with TPs providing the least mixing. Mixing is enhanced at the cost of an increased pressure drop. The area (in top view) of a single RP is 0.075 mm^2, whereas the areas of a single TP and SCP are 0.052 mm^2 and 0.141 mm^2, respectively. Therefore, among the three protrusion designs, constriction of flow cross-sections is maximum for the SCPs. The constriction in flow cross-section forces the streams to come into intimate contact with each other. Apart from possible interpenetration this also causes increased concentration gradient for molecular diffusion leading to enhanced mixing. Periodic flow constriction and expansion also help in mixing. Thus among the protrusions of standard geometrical shapes evaluated in this study, mixing depends mainly on flow constriction. The greater the constriction of the flow, the better the mixing.

As seen from table 1, the mixing index for the microchannel with SCPs is about 5.8 times more than the same in the T-junction microchannel with a straight layout. The pressure drop in the microchannel with SCPs is 11.4 times the

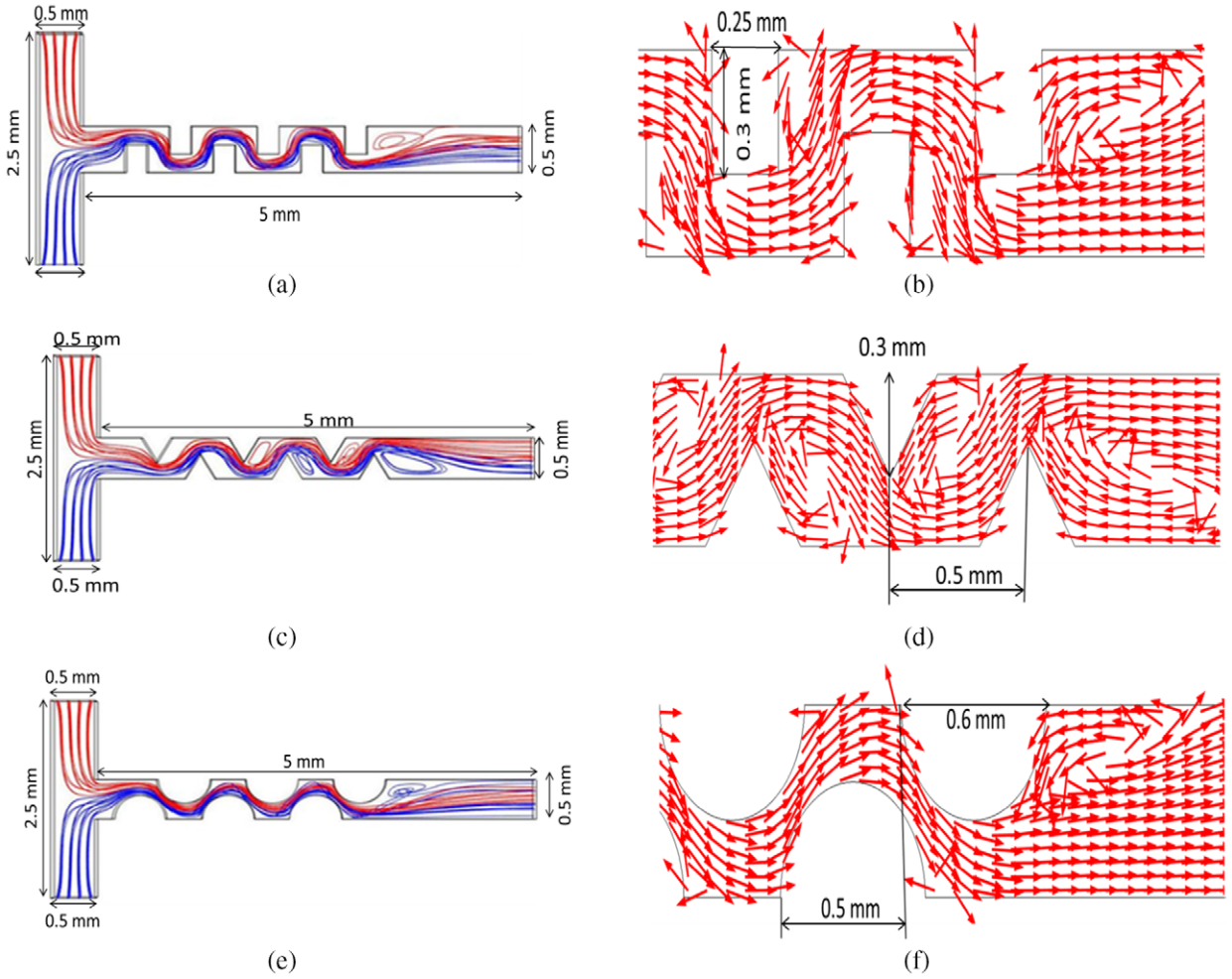

Figure 4. Geometry, streamlines and velocity vectors in T-junction microchannels with inward wall protrusions of different standard geometrical shapes. (a) The geometry of and streamlines in the T-junction microchannel with RPs. (b) The velocity vectors around the RPs. (c) The geometry of and streamlines in the T-junction microchannel with TPs. (d) The velocity vectors around the TPs. (e) The geometry of and streamlines in the T-junction microchannel with SCPs. (f) The velocity vectors around the SCPs.

Table 1. Pressure drop and mixing index for the T-junction microchannels with or without inward wall protrusions of standard geometrical shapes at Re = 50.

Protrusion geometry	ΔP (Pa)	MI (−)	$\Delta P/\Delta P_T$ (−)	MI/MI_T (−)
RP	669	67.6	7.1	5.2
TP	490	63.3	5.2	4.9
SCP	1068	75.1	11.4	5.8
No protrusion	94	12.9	1.0	1.0

pressure drop in the T-junction microchannel with a straight layout. The better mixing in the microchannel with SCPs is thus realized at the cost of an increased pressure drop.

3.2. New shapes of inward wall protrusions

In the designs discussed in the previous section, the enhancement in microfluidic mixing was due to the constriction of the flow cross-section forcing the streams to mix intimately with each other. Mixing can further be enhanced by having protrusions that can superimpose back flow on the bulk flow. This will amount to achieving back mixing in laminar flow and is expected to have a similar effect on mixing as back-mixing induced by eddies in turbulent flow. This idea to improve mixing is evaluated by conceptualizing three designs of inward wall protrusions. The first of these designs is the trapezoidal protrusion (TZP). TZPs have base length of 0.1 mm and a base angle of 120°. The base of the first TZP is at a distance of 1 mm from the junction. Two consecutive TZPs are 0.5 mm apart. The top view and streamlines in the microchannel with an opposed T-junction and six TZPs is shown in figure 6(a). In figure 6(b) the velocity vectors around the TZPs are shown. Another new protrusion design that superimposes backward flow on the forward flow and also causes the flow cross-section to periodically reduce and expand is conceptualized. This protrusion is called the single first bracket protrusion (SFBP). Here, instead of straight reflecting surfaces, curved surfaces are proposed to reflect the flow backwards as curved surfaces can reflect the flow at multiple angles. The SFBP is made of the arcs of two circles each with a radius of 0.3 mm and a center to center distance of 0.1 mm. The centers of both arcs are located at the walls of the microchannel. The first SFBP is located 1 mm away from the microfluidic junction. Two

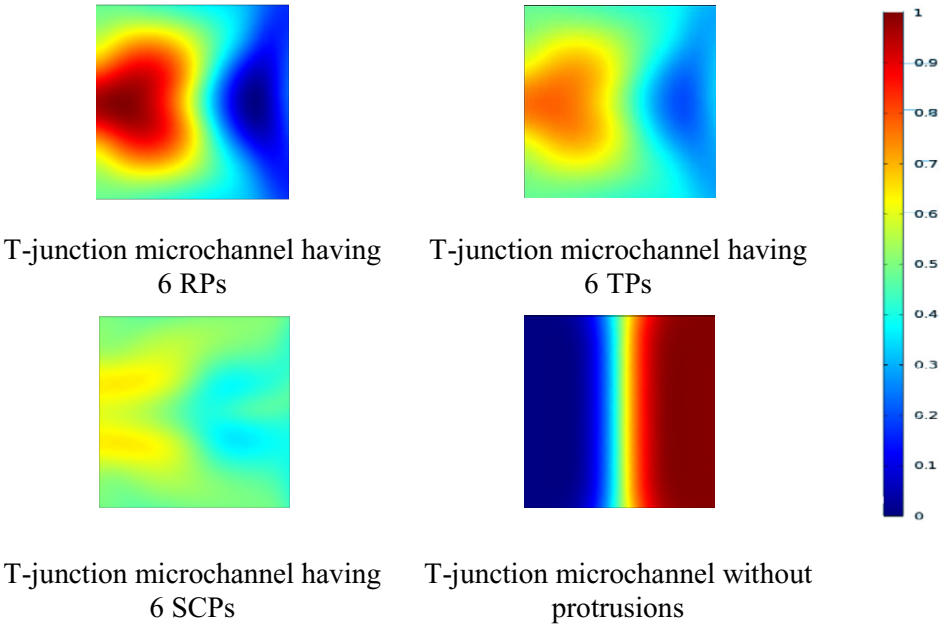

Figure 5. Concentration profiles at the outlets of T-junction microchannels with or without inward wall protrusions of standard geometrical shapes at Re = 50.

adjacent SFBPs are 0.5 mm apart. The top view of a microchannel with an opposed T-junction and six SFBPs is shown in figure 6(c). Figure 6(c) also shows the streamlines in the microchannel with six SFBPs. The stream shown in red hits the second protrusion and flows backward to penetrate the stream shown in blue. This causes some mixing. Then the two streams are forced to pass through a narrow zone between the tips of the first two protrusions. This also causes some mixing. The stream indicated in red hits the fourth protrusion and flows in a backward direction to penetrate the stream indicated in blue. Again, there is narrowing of flow cross-section. This periodically induced backflow followed by passage through a constriction improves mixing significantly. The velocity vectors around SFBPs are shown in figure 6(d). The limitation of SFBPs is that only one of the two streams is made to flow in the backward direction and the backflow is induced only at alternate protrusions, e.g. 2nd, 4th and 6th. To improve this design further a new design of protrusion which induces backflow in both streams is conceptualized and is named the double opposite first bracket protrusion (DOFBP). The shape of the protrusion is similar to the TZP but the non-parallel sides are curved instead of being straight. The protrusion is made by joining the end points of two arcs of circles with radii of 0.3 mm by straight line. This straight line joining the end points of the arcs is parallel to the wall and at distance of 0.3 mm from the wall. The centers of the arcs are on the walls. The distance between the bases of these two arcs emanating from the same wall is 0.1 mm. The base of the first arc is 1 mm from the junction. The distance between two consecutive protrusions (the distance between the end point of the base of one and the start point of the base of the next element) is kept as 0.5 mm. The top view of a microchannel with an opposed T-junction and six DOFBPs is shown in figure 6(e). The streamlines are also shown in figure 6(e). The velocity vectors around the protrusions are shown in figure 6(f). The design of the protrusions is such that backward flow is induced in both streams, e.g. backward flow is introduced in the stream indicated by the red color when it hits the left side of the second protrusion and then the backward flow is induced in the stream indicated by the blue color when it hits the left edge of the third protrusion. The flow is also made to pass through a constricted zone enclosed between the curved surfaces of two adjacent protrusions. This also enhances mixing. The pressure drops and mixing indices at Re = 50 predicted for T-junction microchannels with the new designs of inward protrusions are summarized in table 2. Also listed in table 2 are the pressure drop and mixing index of the microchannel with SCPs which was the best among the microchannels with standard geometrical shapes as wall protrusions. The microchannels with modified designs of protrusions show much better mixing than the microchannels with standard geometrical shapes. The concentration profiles at the outlets of these microchannels are shown in figure 7. The mixing index value for the microchannel with DOFBPs is as high as 94% which is about 20% more than the microchannel with SCPs. The mixing index of the T-junction microchannel with DOFBPs is about 7.3 times larger than the mixing index of a T-junction microchannel with a straight layout. The pressure drop in the T-junction microchannel with DOFBPs is about 54 times greater than the pressure drop in the T-junction microchannel with a straight layout.

3.3. The effect of the Reynolds number

The Reynolds number plays an important role in mixing in microchannels. There are several studies in which the effect of the Reynolds number on mixing has been discussed (Engler *et al* 2004, Kockmann *et al* 2006, Sarkar *et al* 2014). It has also been reported that mixing at low Reynolds numbers is very challenging. A good design of a microchannel for microfluidic mixing should be versatile enough to provide

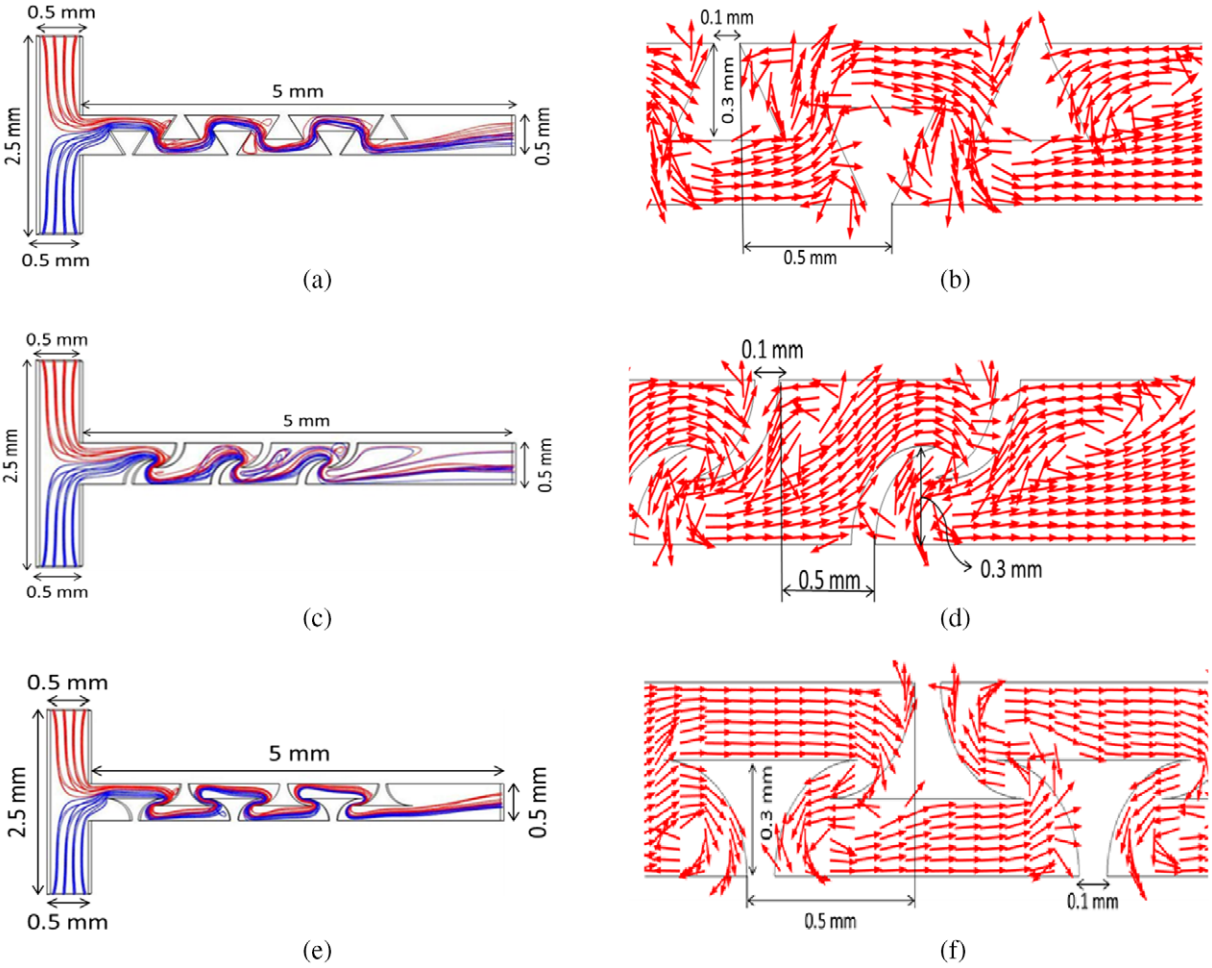

Figure 6. Geometry, streamlines and velocity vectors around protrusions in the microchannels with a T-junction and inward wall protrusions of different new shapes. (a) The geometry of and streamlines in the microchannel with an opposed T-junction with six TZPs. (b) The velocity vectors around the TZPs. (c) The geometry of and streamlines in the microchannel with an opposed T-junction with six SFBPs. (d) The velocity vectors around SFBPs. (e) The geometry of and streamlines in the microchannel with an opposed T-junction and six DOFBPs. (f) The velocity vectors around the DOFBPs.

Table 2. The pressure drop and mixing index for the microchannels with a T-junction and inward wall protrusions of new shapes at Re = 50.

Protrusion geometry	ΔP (Pa)	MI (−)	$\Delta P/\Delta P_T$ (−)	MI/MI_T (−)
TZP	1200	79.7	12.8	6.2
SFBP	2134	88.3	22.7	6.8
DOFBP	5074	94.3	54.0	7.3
SCP	1068	75.1	11.4	5.8

good mixing for a wide range of Reynolds numbers and also at very low Reynolds numbers. Therefore, the designs discussed above are evaluated to determine the kind of mixing these designs provide for a range of Reynolds numbers. To evaluate the effect of the Reynolds number, simulations have been performed for Re = 1 and Re = 100 in addition to Re = 50 for which results have been presented above. Figures 8 and 9 summarize the results obtained from these simulations. As can be seen from figure 8, at Re = 100, the mixing indices in microchannels with protrusions of standard geometrical shapes are comparable with the mixing index in microchannels with new designs of protrusions. However, the mixing indices are not comparable at Re = 1. At Re = 1, the microchannel with DOFBPs stands apart with a mixing index as high as 90. For all the other microchannels, at Re = 1, the mixing index is less than 60.Thus the DOFBPs are the protrusions which ensure good mixing at low as well as at high Reynolds numbers. Figure 9 shows the pressure drop in microchannels for different Reynolds numbers. Although mixing is maximum in the microchannel with DOFBPs, the pressure drop also is maximum in this microchannel. For the lowest Reynolds number (Re = 1) mixing continues to remain almost as high as at the highest Reynolds number, but the pressure drop is significantly lower compared to the pressure drop at the highest Reynolds number. Figure 10 shows the concentration contours at the outlets of opposed T-junctions with SCPs, SFBPs and DOFBPs for three different Reynolds numbers. Unlike the microchannels with SCPs and SFBPs, almost uniform mixing can be seen at the outlet of the microchannel with DOFBPs for all values of Reynolds numbers.

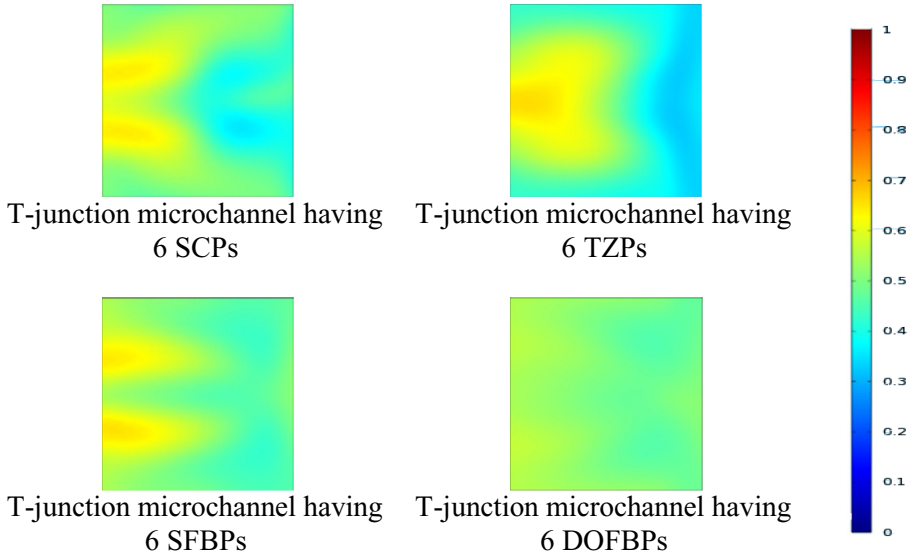

Figure 7. The concentration profiles at the outlets of the opposed T-junction microchannels with inward wall protrusions of different shapes at Re = 50.

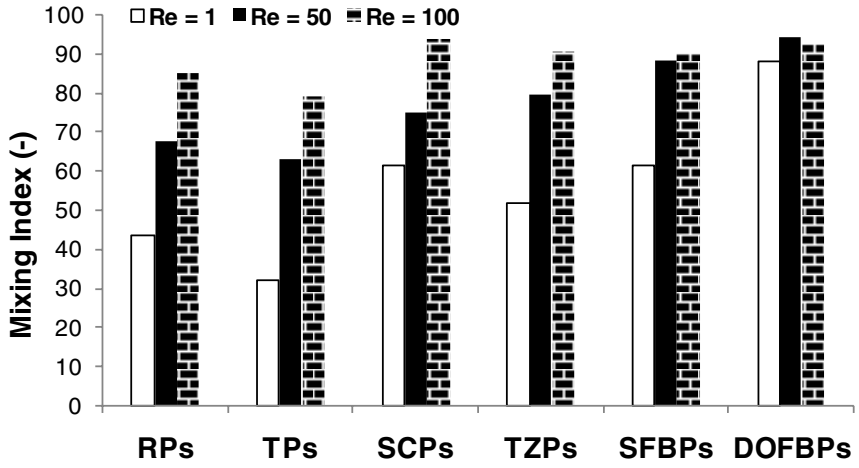

Figure 8. Comparison of the mixing index at the outlets of the microchannels with opposed T-junctions with different types of inward wall protrusions.

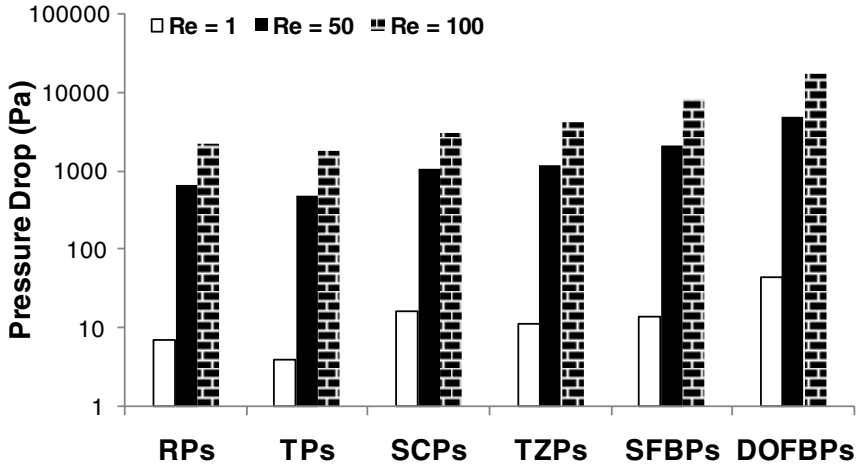

Figure 9. Comparison of the pressure drop in the microchannels with opposed T-junction and different types of inward wall protrusions.

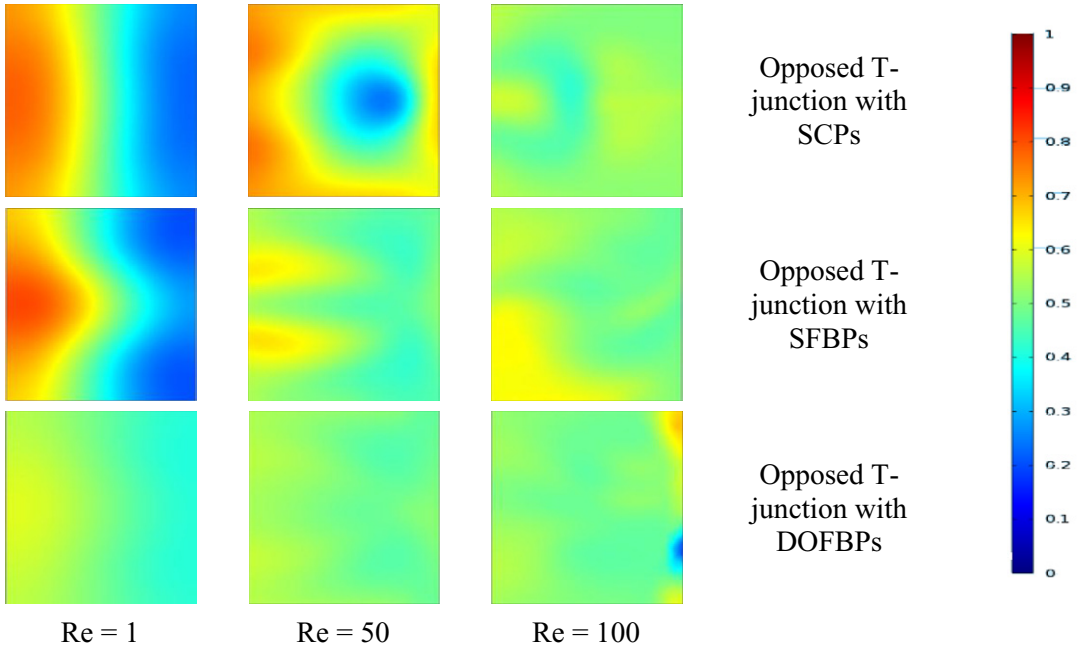

Figure 10. Concentration profiles at the outlets of the microchannels with an opposed T-junction with different types of wall protrusions at Re = 1, 50 and 100.

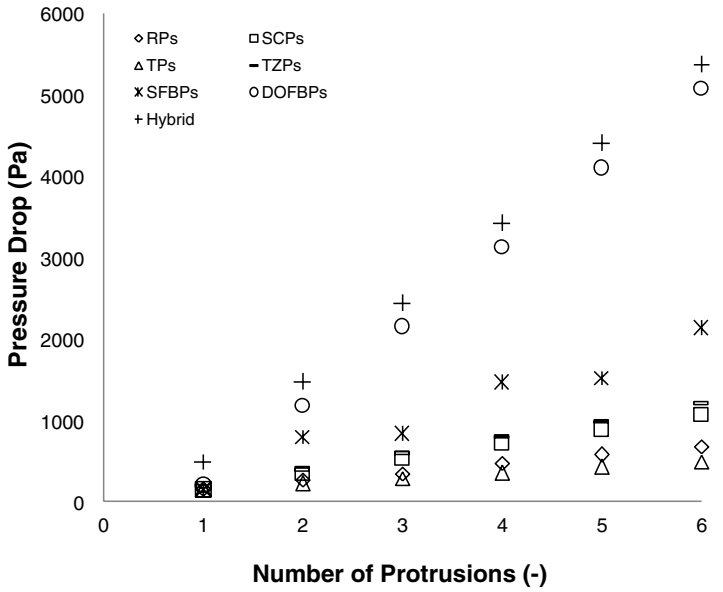

Figure 11. Variation of the pressure drop with the number of protrusions at Re = 50.

3.4. The effect of the number of protrusions

All the microchannels discussed in the previous sections had six protrusions. As the number of protrusions increases, the mixing index and pressure drop are both expected to increase. However, with a continued increase in the number of protrusions, while the pressure drop continues to increase, the mixing index will eventually tend to become constant. Thus it is important to know the effect of the number of protrusions on the mixing index and the pressure drop so that the optimum number of protrusions can be decided. To study the effect of the number of protrusions, simulations were carried out considering microchannels with 1–6 protrusions. The pressure drop and mixing index values obtained from the simulations are plotted in figures 11 and 12. Figures 11 and 12 also contain the data of the microchannel based on the hybrid concept of increasing microfluidic mixing. This will be discussed in the following section. It can be noted from figure 12 that for protrusions of standard geometrical shapes, the mixing index continues to increase when the number of protrusions is increased from one to six. But in the case of DOFBPs the mixing index does not increase much after the 4th or 5th protrusion. So if a microchannel with DOFBPs is to be used, four or five protrusions are sufficient.

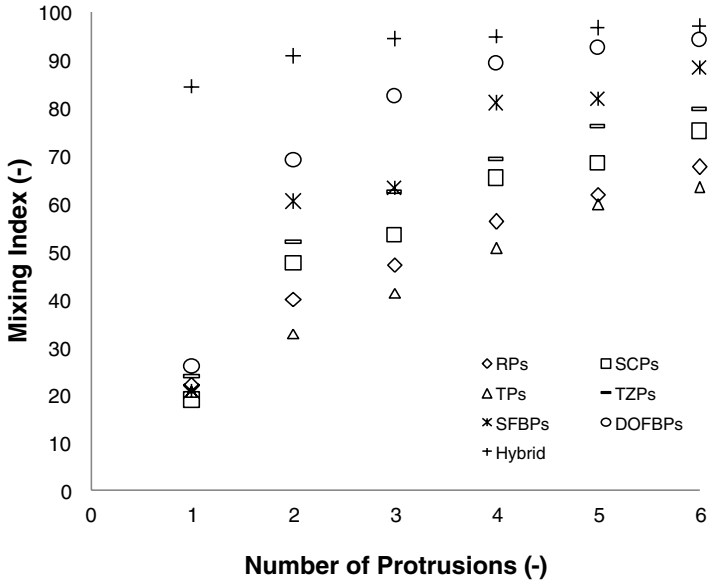

Figure 12. Variation of the mixing index with the number of protrusions at Re = 50.

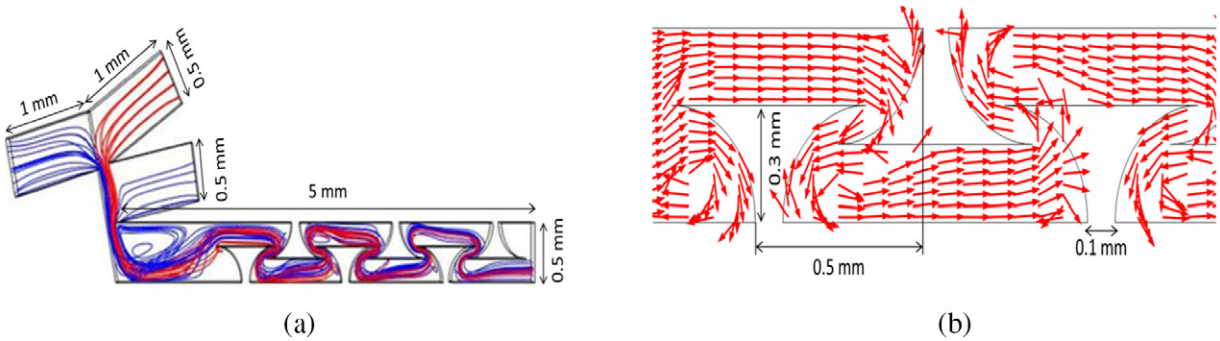

Figure 13. (a) Geometry of and streamlines in the microchannel with an OA 10°–20°–165° WY-junction with six DOFBPs. (b) The velocity vectors around the protrusions.

3.5. The hybrid approach for enhancing microfluidic mixing

The approach of providing inward wall protrusions in a T-junction microchannel to improve mixing can be called a simple-junction–complex-layout approach to improve microfluidic mixing. The other approach to improve microfluidic mixing is a complex-junction–simple-layout approach in which changes are made at the microfluidic junction keeping the layout straight. The complex-junction–simple-layout approach was the subject of our previous study in which a microfluidic junction called the OA 10°–20°–165° WY-junction was found to provide the best mixing among all the microfluidic junctions that were evaluated (Sarkar *et al* 2014). To further improve the mixing in a microchannel a hybrid approach can be contemplated. The hybrid approach will involve modification of both the junction and layout and hence can be called a complex-junction–complex-layout approach to enhance microfluidic mixing. Combining the best microfluidic junctions identified in our previous study and the best geometry of protrusions identified in this study, a microchannel with an OA 10°–20°–165° WY-junction and DOFBPs is conceptualized and evaluated. Six protrusions are considered. The Reynolds numbers for which simulations are carried out are 1, 50 and 100. The geometry and streamlines in the microchannel with an OA 10°–20°–165° WY-junction with six DOFBPs are shown in figure 13(a) and the velocity vectors around the protrusions are shown in figure 13(b). The mixing indices and pressure drops estimated for different Reynolds numbers are summarized in table 3. As can be seen from table 3, the microchannel based on the hybrid approach to enhance microfluidic mixing has a mixing index as high as 94.2 for Re = 1.

Table 3. The mixing index and pressure drop in the microchannel with an OA 10°–20°–165° WY-junction with six DOFBPs at different Reynolds numbers.

Reynolds number	ΔP(Pa)	MI (−)	$\Delta P/\Delta P_T$ (−)	MI/MI_T (−)
1	46	94.2	25.7	5.0
50	5369	97.2	54.0	7.3
100	18 980	96.7	84.0	5.6

The mixing index and pressure drop values obtained from simulations at Re = 50 are summarized in table 4 along with the mixing index and pressure drop in an OA 10°–20°–165° WY-junction with a straight layout, representative of the complex-junction–simple-layout approach, and a T-junction microchannel with six DOFBPs, representative of the

Table 4. Comparison of the microchannel with an OA 10°–20°–165° WY-junction with six DOFBPs, the microchannel with an OA 10°–20°–165° WY-junction with a straight layout and an opposed T-junction with six DOFBPs at Re = 50.

Type of microchannel	Pressure drop (Pa)	MI (−)	$\Delta P/\Delta P_T$ (−)	MI/MI_T (−)
OA 10°–20°–165° WY-junction with straight layout	340	86.4	3.6	6.7
Opposed T-junction with six DOFBPs	5074	94.3	54.0	7.3
OA 10°–20°–165° WY-junction with six DOFBPs	5369	97.2	57.1	7.5

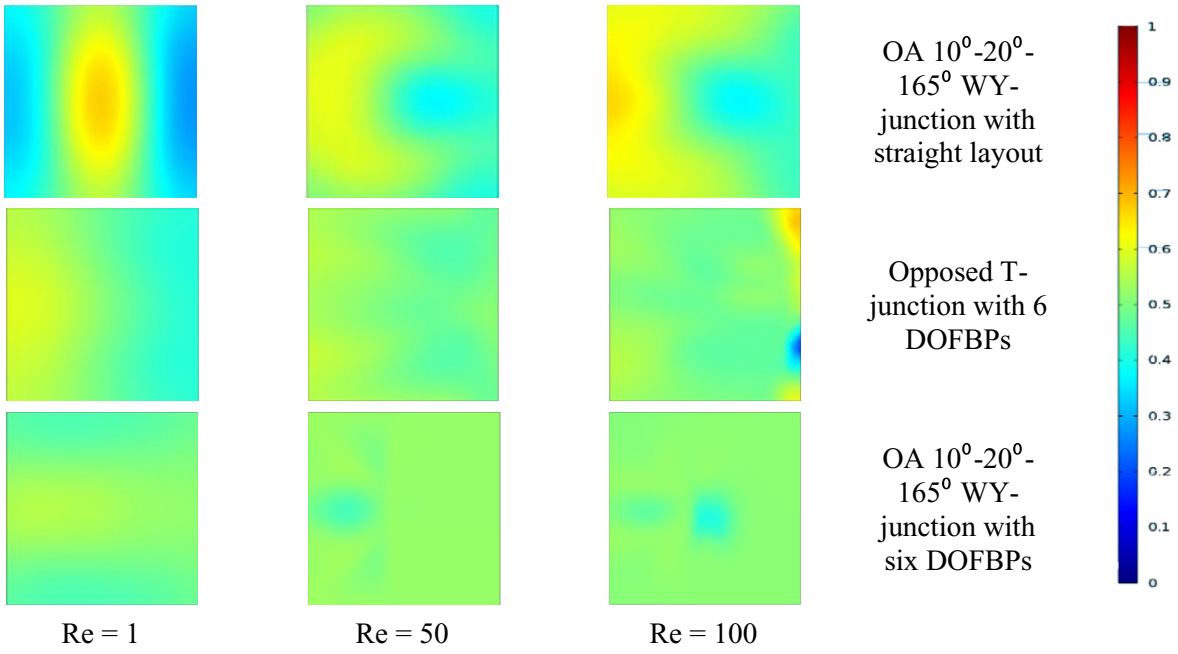

Figure 14. Concentration contours at the outlets of an OA 10°–20°–165° WY-junction with a straight layout, an opposed T-junction with six DOFBPs and an OA 10°–20°–165° WY-junction with six DOFBPs at different Reynolds numbers.

simple-junction–complex-layout approach. A comparison of the concentration contours at the outlets of these three microchannels is shown in figure 14. As can be seen the microchannel based on the hybrid approach provides better mixing than the microchannels based on the complex-junction–simple-layout approach or simple-junction–complex-layout approach. The simple-junction–complex-layout approach is observed to be better than the complex-junction–simple-layout approach.

As discussed earlier, identifying the optimum number of protrusions is important to achieve high mixing with the minimum possible pressure drop. Therefore, simulations were carried out to estimate the mixing index and pressure drop in the microchannel based on the hybrid approach considering different number of protrusions. The results are shown in figures 11 and 12. For Re = 50 the mixing index increases only marginally when the number of protrusions is increased from three to six but the pressure drop increases significantly. Therefore, the microchannel with an OA 10°–20°–165° WY-junction and three DOFBPs is found to be the optimum geometry based on the hybrid approach to improve microfluidic mixing.

3.6. The comparison with a T-junction microchannel with a straight layout for the same mixing index

In the microchannel designs proposed above the pressure drop is apparently high. For example, the microchannel with an opposed T-junction and six DOFBPs has a mixing index of 94.3 but a pressure drop of 5074 Pa at Re = 50. The pressure drop in the microchannel with an opposed T-junction and six DOFBPs is thus about 54 times more than the pressure drop in the T-junction microchannel with a straight layout. Similarly, the microchannel based on the hybrid approach with an OA 10°–20°–165° WY-junction and six DOFBPs gives a mixing index of 97.2 but a pressure drop of 5369 Pa at Re = 50. The pressure drop in the microchannel based on the hybrid approach is thus about 57 times more than the pressure drop in the T-junction microchannel with a straight layout. Thus one may have the view that the mixing index is enhanced in the new designs at the expense of substantially increased pressure drop and hence the new designs are no better than conventional microchannels. However, the basis of comparison should be the pressure drop for the same mixing index. The data from the numerical simulations of the opposed T-junction without any protrusions were used to estimate the length required to obtain the same mixing index as in the microchannel with an opposed T-junction with DOFBPs at Re = 50. The length required is estimated to be 770 mm and the corresponding pressure drop at Re = 50 as 9087 Pa, which is about twice that of the pressure drop in the microchannel with an opposed T-junction with DOFBPs. The volume of the opposed T-junction with DOFBPs is 1.875 mm^3. The volume of the microchannel with an opposed T-junction without

protrusions but providing the same mixing index as the microchannel with an opposed T-junction with DOFBPs will be a whopping 193.125 mm^3. Thus, if we use a microchannel with an opposed T-junction without protrusions to target very high mixing, the pressure drop will be very high and so will be the inventory locked in the microchannel, thus defeating the very concept of miniaturization. Thus, the proposed designs are distinctly better than the conventional designs for microfluidic mixing.

4. Conclusion

Computational fluid dynamics simulations are used to explore the possibility of enhancing microfluidic mixing by modifying the layout of microchannels. Specifically, the effect of inward wall protrusions on microfluidic mixing is investigated. Opposed T-junctions with inward wall protrusions of standard geometrical shapes such as rectangles, triangles and semicircles, are evaluated. Among these standard geometrical shapes the semicircular protrusions are found to provide the best mixing. Several new designs of inward wall protrusions are also conceptualized and evaluated. Among these a design called the double opposite first bracket protrusion (DOFBP) is found to provide very good mixing. The microchannel having opposed T-junction having DOFBPs is found to provide very good mixing for a wide range of Reynolds numbers. A microchannel based on the hybrid approach for improving microfluidic mixing is also evaluated. This microchannel combines an OA 10°–20°–165° WY-junction and DOFBPs to provide very high mixing. The performance of this microchannel based on the hybrid approach to improve microfluidic mixing is found to be better than the microchannel comprising an opposed T-junction with DOFBPs. For the same mixing index, the pressure drop and volume of the opposed T-junction with a straight layout are estimated to be much higher than the pressure drop and volume of the proposed new designs. This highlights the possibility of significant intensification of microfluidic mixing by using the proposed new designs with inward wall protrusions.

Acknowledgment

SS is thankful to the Department of Atomic Energy, India for providing a fellowship under DAE Graduate Fellowship Scheme.

References

Adeosun J T and Lawal A 2009 Numerical and experimental studies of mixing characteristics in a T-junction microchannel using residence-time distribution *Chem. Eng. Sci.* **64** 2422–32

Afzal A and Kim K Y 2014 Flow and mixing analysis of non-Newtonian fluids in straight and serpentine microchannels *Chem. Eng. Sci.* **116** 263–74

Alam A and Kim K-Y 2012 Analysis of mixing in a curved microchannel with rectangular grooves *Chem. Eng. J.* **181–2** 708–16

Bhoi R *et al* 2014 Transesterification of sunflower oil in microreactors *Int. J. Chem. React. Eng.* **12** 47–62

Bothe D, Stemich C and Warnecke H J 2006 Fluid mixing in a T-shaped micro-mixer *Chem. Eng. Sci.* **61** 2950–58

Capretto L, Cheng W, Hill M and Zhang X 2011 Micromixing within microfluidic devices *Top. Curr. Chem.* **304** 27–68

Cvjetko M and Žnidaršič-Plazl P 2011 Ionic liquids within microfluidic devices *Ionic Liquids: Theory, Properties, New Approaches* (Rijeka: InTech) pp 681–700

Darekar M *et al* 2014a Liquid–liquid extraction in microchannels with Zinc-D2EHPA system *Hydrometallurgy* **144–145** 54–62

Darekar M *et al* 2014b Extraction of uranium from dilute solution using microbore tube *BARC Newsl.* **338** 9–14

de Mello A J *et al* 2004 Precise temperature control in microfluidic devices using Joule heating of ionic liquids *Lab Chip* **4** 417–19

Dipprey D F and Sabersky R H 1963 Heat and momentum transfer in smooth and rough tubes at various Prandtl numbers *Int. J. Heat Mass Transfer* **6** 329–32

Engler M, Kockmann N, Kiefer T and Woias P 2004 Numerical and experimental investigations on liquid mixing in static micromixers *Chem. Eng. J.* **101** 315–22

Fang Y *et al* 2012 Mixing enhancement by simple periodic geometric features in microchannels *Chem. Eng. J.* **187** 306–10

Gee D L 1980 Forced convection heat transfer in helically rib-roughened tubes *Int. J. Heat Mass Transfer* **23** 1127–36

Glasgow I and Aubry N 2003 Enhancement of microfluidic mixing using time pulsing *Lab Chip* **3** 114–20

Hessel V *et al* 2005 Aqueous Kolbe–Schmitt synthesis using resorcinol in a microreactor laboratory rig under high-*p*, *T* conditions *Org. Process Res. Dev.* **9** 479–89

Iwasaki T, Kawano N and Yoshida J I 2006 Radical polymerization using microflow system: numbering-up of microreactors and continuous operation *Org. Process Res. Dev.* **10** 1126–31

Kikutani Y *et al* 2002 Pile-up glass microreactor *Lab Chip* **2** 193–6

Khodadadi J M, Nguyen T M and Vlachos N S 1986 Laminar forced convective heat transfer in a 2D 90° bifurcation *Numer. Heat Transfer* **9** 677–95

Kockmann N, Kiefer T, Engler M and Woias P 2006 Convective mixing and chemical reactions in microchannels with high flow rates *Sensors Actuators* **117** 495–508

Leung, W W F and Ren Y 2013 Crossflow and mixing in obstructed and width-constricted rotating radial microchannel *Int. J. Heat Mass Transfer* **64** 457–67

Liu M 2011 Computational study of convective–diffusive mixing in a microchannel mixer *Chem. Eng. Sci.* **66** 2211–23

Mengeaud V, Josserand J and Girault H H 2002 Mixing processes in a zigzag microchannel: finite element simulations and optical study *Anal. Chem.* **74** 4279–86

Nguyen N T and Wu Z 2005 Micromixers—a review *J. Micromech. Microeng.* **15** R1

Nguyen T M, Khodadadi J M and Vlachos N S 1989 Laminar flow and conjugate heat transfer in rib roughened tubes *Numer. Heat Transfer Part* A **15** 165–79

Nonino C, Savino S and Del Giudice S 2009 Numerical assessment of the mixing performance of different serpentine microchannels *Heat Transfer Eng.* **30** 101–12

Oddy M, Santiago J and Mikkelsen J 2001 Electrokinetic instability micromixing *Anal. Chem.* **73** 5822–32

Ottino J M and Wiggins S 2004 Introduction: mixing in microfluidics *Phil. Trans. R. Soc.* A **362** 923–35

Saber M, Commenge J M and Falk L 2010 Microreactor numbering-up in multi-scale networks for industrial-scale applications: impact of flow maldistribution on the reactor performances *Chem. Eng. Sci.* **65** 372–9

Sahu P K, Golia A and Sen A K 2013 Investigations into mixing of fluids in microchannels with lateral obstructions *Microsyst. Technol.* **19** 493–501

Sarkar S, Singh K K, Shankar V and Shenoy K T 2014 Numerical simulation of mixing at 1–1 and 1–2 microfluidic junctions *Chem. Eng. Process.* **85** 227–40

Sen N *et al* 2014 Solvent extraction and stripping studies in microchannels with TBP nitric acid system *Solvent Extr. Ion Exc.* **32** 281–300

Sen N *et al* 2013 Continuous, solvent free, high temperature synthesis of ionic liquid 1-butyl-3-methylimidazolium bromide in a microreactor *BARC Newsl.* **334** 20–3

Sheu T S, Chen S J and Chen J J 2012 Mixing of a split and recombine micromixer with tapered curved microchannels *Chem. Eng. Sci.* **71** 321–32

Soleymani A, Kolehmainen E and Turunen I 2008 Numerical and experimental investigations of liquid mixing in T-type micromixers *Chem. Eng. J.* **135** S219–28

Suh Y K and Kang S 2010 A review on mixing in microfluidics *Micromachines* **1** 82–111

Wang L, Ma S and Han X 2015 Micromixing enhancement in a novel passive mixer with symmetrical cylindrical grooves *Asia-Pac. J. Chem. Eng.* **10** 201–9

Waterkamp D A *et al* 2007 Synthesis of ionic liquids in micro-reactors—a process intensification study *Green Chem.* **9** 1084–90

Webb R L 1971 Heat transfer and friction in tubes with repeated-rib roughness *Int. J. Heat Mass Transfer* **14** 601–17

Wong S H, Bryant P, Ward M and Wharton C 2003 Investigation of mixing in a cross-shaped micromixer with static mixing elements for reaction kinetics studies *Sensors Actuators* **95** 414–24

Wong S H, Ward M C and Wharton C W 2004 Micro T-mixer as a rapid mixing micromixer *Sensors Actuators* **100** 359–79

Yaralioglu G, Wygant I, Marentis T and Khuri-Yakub B 2004 Ultrasonic mixing in microfluidic channels using integrated transducers *Anal. Chem.* **76** 3694–98

Yue J *et al* 2007 Hydrodynamics and mass transfer characteristics in gas–liquid flow through a rectangular microchannel *Chem. Eng. Sci.* **62** 2096–108

Zhao Y, Chen G and Yuan Q 2007 Liquid–liquid two-phase mass transfer in the T-junction microchannels *AIChE J.* **53** 3042–53